

Donor–Acceptor Pair Quantum Emitters in Hexagonal Boron Nitride

Qinghai Tan,[○] Jia-Min Lai,[○] Xue-Lu Liu, Dan Guo, Yongzhou Xue, Xiuming Dou, Bao-Quan Sun, Hui-Xiong Deng, Ping-Heng Tan, Igor Aharonovich,^{*} Weibo Gao,^{*} and Jun Zhang^{*}



Cite This: *Nano Lett.* 2022, 22, 1331–1337



Read Online

ACCESS |



Metrics & More



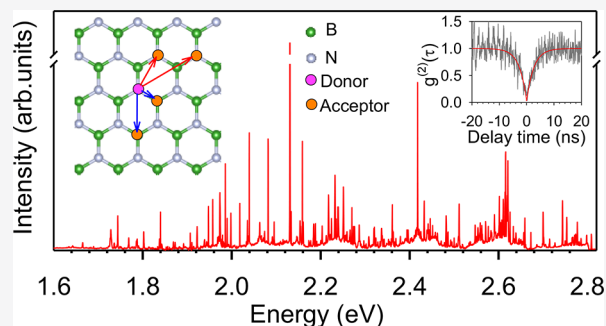
Article Recommendations



Supporting Information

ABSTRACT: Quantum emitters are needed for a myriad of applications ranging from quantum sensing to quantum computing. Hexagonal boron nitride (hBN) quantum emitters are one of the most promising solid-state platforms to date due to their high brightness and stability and the possibility of a spin–photon interface. However, the understanding of the physical origins of the single-photon emitters (SPEs) is still limited. Here we report dense SPEs in hBN across the entire visible spectrum and present evidence that most of these SPEs can be well explained by donor–acceptor pairs (DAPs). On the basis of the DAP transition generation mechanism, we calculated their wavelength fingerprint, matching well with the experimentally observed photoluminescence spectrum. Our work serves as a step forward for the physical understanding of SPEs in hBN and their applications in quantum technologies.

KEYWORDS: Hexagonal Boron Nitride, Single-Photon Emitters, Donor–Acceptor Pairs, Quantum Optics



INTRODUCTION

Layered van der Waals materials have received much attention not only for their novel optoelectronic properties^{1,2} but also for their capability of hosting a wealth of optically active defects that act as single-photon emitters (SPEs).^{3,4} In particular, SPEs from 2D hexagonal boron nitride (hBN) exhibit stable, bright, and efficient emission into the zero-phonon line (ZPL), even at ultrahigh temperatures.^{4–12} Furthermore, the spin information on these emitters serves as a promising platform for fundamental research and potential applications in quantum technologies.^{13–15} However, the origin and the nature of the hBN SPEs remain under debate.^{16–19} The emission spectra of both intrinsic and engineered defects in hBN show a broadband spectral range, distinct polarization profiles, and different quantum efficiencies.^{10,16,17,19} Several bottom-up growth techniques and postprocessing approaches such as ion implantation or electron irradiation have been aimed at identifying the sources.^{14,20–22} In addition, multiple theoretical calculations show that different types of atomic defects may exist, including nitrogen or boron vacancy complexes, antisite defects, and substitutional defects with carbon or oxygen,^{16,17,19,23–26} but conclusive evidence of these prediction results is still lacking.

As one of the fluorescence mechanisms, the donor–acceptor pair (DAP) transition between ionized donors and acceptors has been studied in traditional semiconductors, including silicon,^{27,28} silicon carbide,^{29,30} diamond,³¹ and other compound semiconductors.^{32–35} In general, the DAP transition is characterized by a series of sharp photoluminescence (PL) lines with a broadband wavelength range at low temper-

atures.^{28–31} In particular, designing the emitters with a well-defined donor–acceptor distance and orientation in covalently linked organic molecules can enable a promising avenue for the manipulation and coherent control of spin states.^{36,37} Recently, DAP-induced emission has been theoretically predicted in hBN.³⁸

Here we present experimental evidence of the existence of DAP quantum emitters in hBN. At low temperatures, we observe dense sharp PL lines over a broad range of wavelengths from blue (~440 nm) to red (~800 nm) color. On the basis of the DAP transition mechanism, we use the DAP model to calculate the emission lines, matching the experimental results very well. We also give the possible origin of the DAP by comparing fitting results and density functional theory (DFT) calculations. Our work indicates that the DAP transition mechanism may explain the broad distribution of observed quantum emitters in hBN and serve as a foundation for designing scalable quantum devices.

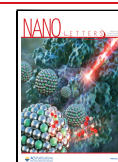
DAP TRANSITION IN hBN

The DAP transition describes a fluorescence mechanism that includes the Coulomb interaction between the ionized donors

Received: December 1, 2021

Revised: January 14, 2022

Published: January 24, 2022



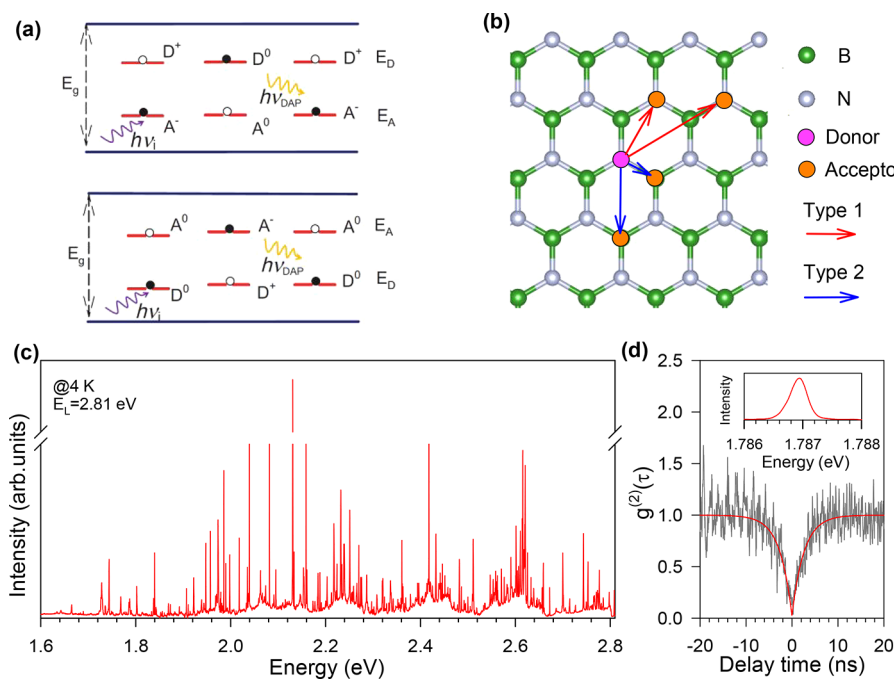


Figure 1. (a) Schematic diagram of the DAP transitions in large-band-gap semiconductors. (b) Diagram of *type 1* (red arrow) and *type 2* (blue arrow) DAP transitions in hBN. (c) PL spectrum of one typical hBN sample with 442 nm (2.81 eV) laser excitation at 4 K. (d) Measurement result of the second-order correlation function for one PL peak at 4 K. The inset shows the corresponding PL spectrum.

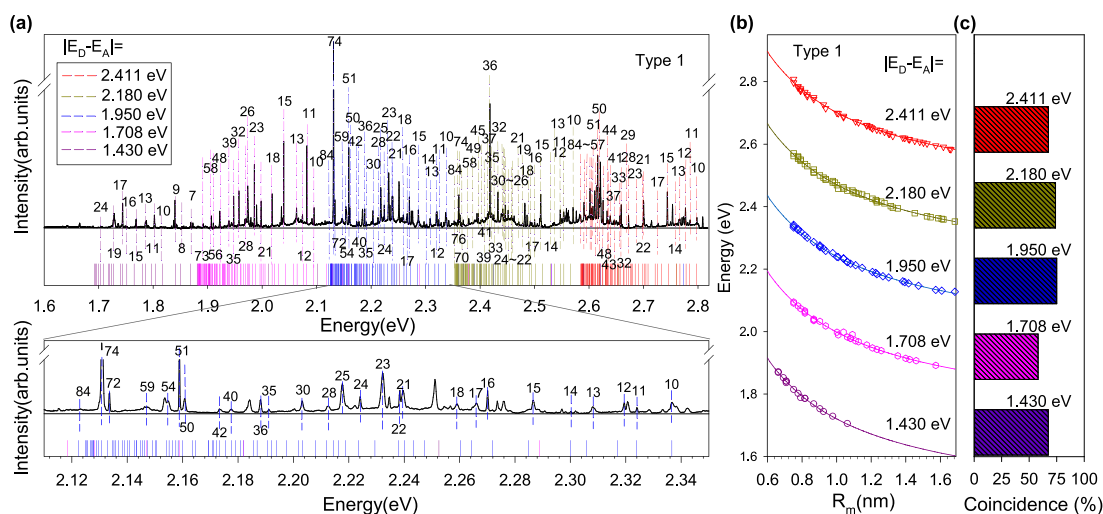


Figure 2. (a) Calculated spectral distribution of *type 1* DAPs (color solid lines). The solid black line is the measured spectrum at 4 K. The labeled numbers of the peaks are the shell numbers for the neighboring DA pairs, and the dashed lines are used to guide the eyes. Here 2.411 eV and so on represent the energy levels for $|E_D - E_A|$. The bottom part shows a zoomed-in range in the upper part. (b) Calculated emitted-photon energies are based on the DAP model as a function of R_m (the distance between the donors and acceptors, where m is the shell number). The solid symbols are experimental results, and the solid curves are the calculated results of *type 1* based on eq 1. (c) Coincidence of experimental lines that match the calculated DAP lines over all measured PL lines in each range.

and acceptors. Considering the nature of deep levels in the wide band gap of semiconductors (e.g., hBN), the DAP transition process can be simply described as follows: The electrons (holes), created by laser excitations, can be trapped by the ionized donor sites (D^+) (or the neutral A^0) and acceptor sites (A^-) (or the neutral D^0) before the radiative recombination and the photon emissions, as shown in Figure 1a. In general, two types of DAP transitions exist considering the random distribution of D^+ and A^- sites: *type 1*, where both donors and acceptors are located at the same atomic element species, as illustrated by the red arrows in Figure 1b, and *type 2*,

where the donors and acceptors occupy different atom sites, as indicated by the blue arrows in Figure 1b. This radiative recombination of DAPs in semiconductors can generate a series of sharp lines with a broadband distribution in the PL spectra, as reported for other semiconductors.^{27–30,32–35}

Figure 1c shows the typical PL spectrum of single-photon emitters from an hBN sample at 4 K. The hBN samples are prepared on SiO_2/Si substrate from hBN flakes suspended in 50/50 ethanol/water solution (Graphene Supermarket). More experimental results can be found in Supporting Information Figure S1. Interestingly, we found that the spectrum shows

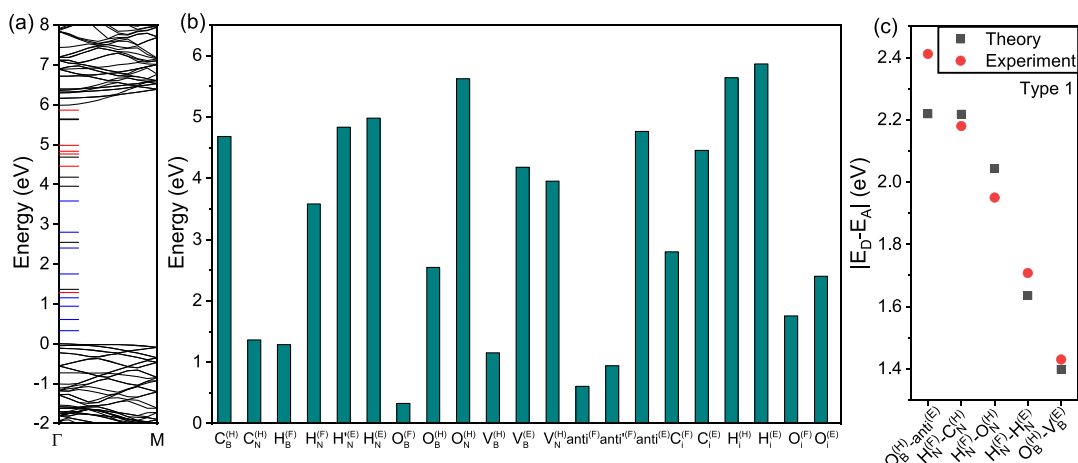


Figure 3. (a) Calculated band structure of bulk hBN and the energy levels of different defect types. The blue lines indicate the defect states that are fully filled with electrons, the black straight lines represent the defect states that are half-filled with electrons, and the red lines denote the empty defect states. The energy of the host valence band maximum is set to zero. (b) Energy of different defect types. The superscripts (F), (H), and (E) indicate that the defect states are fully filled with electrons, half-filled with electrons, and empty, respectively. (An apostrophe (') is used to distinguish some substitutional atoms with the same electron occupancy of two energy levels.) For example, $C_B^{(H)}$ denotes a C impurity substituting for a lattice B atom and half-filled with electrons. Antisite denotes B_N and N_B , and V_B and C_i denote a boron vacancy and carbon interstitial, respectively. (c) $|E_D - E_A|$ of different *type 1* DAPs from our fitting result (red circle) and DFT calculation (black square).

dense sharp emission lines and covers a wide energy range from 2.80 (443 nm) to 1.544 eV (803 nm), confirmed on multiple samples (Figure S1). Furthermore, these lines also show a narrow line width down to ~ 75 μ eV, as shown in Figure S1, which is close to the narrowest line width of quantum emitters in hBN currently reported.⁹ Figure 1d and Figure S2 shows the $g^{(2)}(\tau)$ measurement results of two randomly selected PL lines, which prove that they are single-photon emitters. We also measured the stability of PL lines at different emission wavelengths and found that they are stable and bright, as shown in Figure S3.

On the basis of the DAP transition mechanism, we used the theoretical DAP model that follows to calculate the emission lines. In this model, the electrons, instead of relaxing from the valence band to donors or acceptors, as reported in previous studies, such as in GaP,^{33–35} relax between defect levels within the large band gap of hBN. Thus the energy of the emitted photons can be written as³³

$$E(R_m) = |E_D - E_A| + \frac{e^2}{4\pi\epsilon\epsilon_0 R_m} \quad (1)$$

where E_A and E_D are the donor and acceptor levels, respectively. R_m is the m th ($m = 1, 2, 3, \dots$) nearest distance between the donors and acceptors, as determined by the crystal structure and lattice constant, and m is the shell number. $\frac{e^2}{4\pi\epsilon\epsilon_0 R_m}$ describes the Coulomb interaction between the donor and acceptor. The discrete R_m in the Coulomb term is responsible for the observed sharp lines in the emission spectra. For large R_m , the lines are closely located and barely distinguishable, resulting in a broad peak. Figure 2a shows the calculated spectral distributions and the zoom-in result for *type 1* DAPs based on five different $|E_D - E_A|$ values. (Other zoom-in results are shown in Figure S4.) To further confirm the rationality of the model, we used a series of values that slightly deviate from one $|E_D - E_A|$ to calculate the DAP lines, as shown in Figure S5, and found that these calculated lines cannot match well with the experimental lines, especially for small m numbers. Moreover, we also found that these

calculated DAP lines based on the same $|E_D - E_A|$ values match well with the experimental results from other samples, as shown in Figure S6. These results indicate that these sharp hBN PL lines here are indeed from the DAP process.

Figure 2b shows the calculated emitted-photon energies of the DAP as a function of R_m between the donors and acceptors. We found that the calculated results match most of the PL lines. Remarkably, we found that $\sim 70\%$ of the theoretically calculated emission wavelengths match precisely the experimental results, as shown in Figure 2c, indicating the truth of the DAP mechanism here. The unmatched lines can be attributed to the inhomogeneous distribution of the defects and the multipole term.²⁹ In addition, the crystal structure of the hBN sample may be deformed with strain, which can also lead to small deviations.³⁴ Meanwhile, some of the emission lines may originate directly from the color centers without DAP effects. As shown in Figure S7, our results suggest that both of the two types of DAP transitions may coexist in our hBN samples due to random doping. The lifetimes of different DAP lines are also measured, as shown in Figure S8, and they become longer as the shell number increases. These results can be understood by considering that the wave functions between electrons and holes in the DAP is reduced with the R_m increase, and thus the lifetime is slightly changed.³⁴ The weak lifetime dependence on shell number can be understood by considering the deep-level nature of hBN, the small varied R_m (0.7 to 1.6 nm) here, and the relatively large exciton Bohr radius (on the order of a few nanometers) of Wannier exciton type in 2D materials.¹ More detailed discussions can be found in the Supporting Information. Considering that the DAP line here depends only on the defect concentration, defect types, and lattice structure, the SPEs induced by the DAP mechanism are also expected to be observed for hBN samples prepared by other methods, such as chemical vapor deposition (CVD)-grown hBN and strain-engineered hBN.

To understand the original defect of the DAP, we calculated the electronic energy band structures of the bulk hBN and its possible defect states (Figure 3) based on DFT. At 4 K, the electron–phonon coupling is weak (almost no phonon

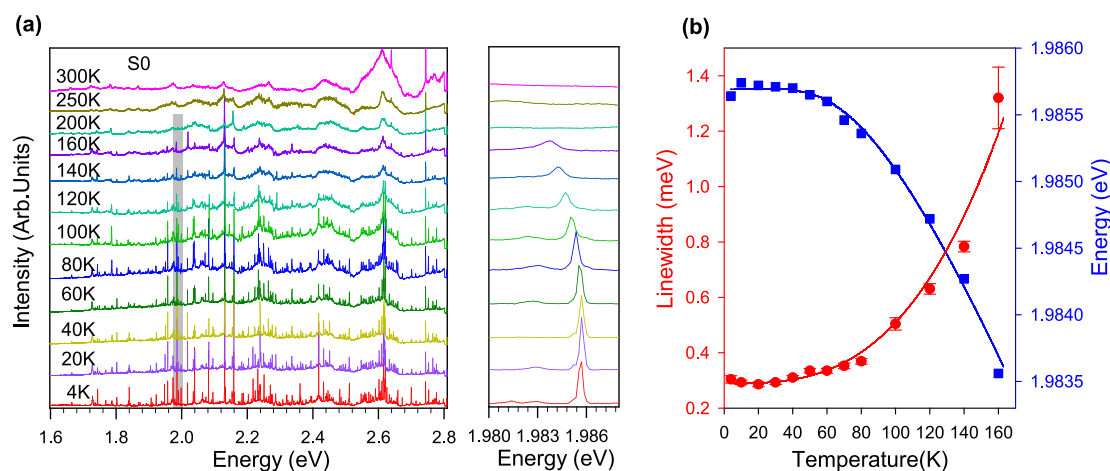


Figure 4. (a) Temperature-dependent spectra of hBN SPEs excited by 442 nm (2.81 eV) from 4 to 300 K. The peak at 1.9856 eV (the shadow region) is zoomed-in as an example. (b) Temperature dependence of the line width and energy of the PL peak at 1.9856 eV (4 K). The red solid line in panel b is fitted by the function $aT^\alpha + b$, where $a = 2.21 (0.16) \times 10^{-10}$, $\alpha = 3.00 (0.02)$, and $b = 2.89 (0.07) \times 10^{-4}$ eV. The energy of ZPL is fitted by the O'Donnell equation (blue line) $E(T) = E(0) - S <\hbar\omega> \coth[\hbar\omega/2k_B T]$, where S is an exciton–phonon coupling constant and $<\hbar\omega>$ is the average phonon energy. Here $E_g(0)$, S , and $<\hbar\omega>$ are around 1.99 eV, 0.20, and 24.61 meV, respectively.

sideband is observed in our spectra), and the lattice relaxation hardly affects the calculation of defect energy levels, and thus we did not consider the lattice relaxation.¹⁶ The calculated band gap of bulk hBN is 5.98 eV, which is consistent with previous experimental results.³⁹ We considered all possible transitions based on the DFT-calculated level of defects, that is, the electron transition from the fully filled or half-filled level to the half-filled or empty level, and got the transition energy by the energy difference between these levels. Comparing with the fitting results, we listed the possible origin of DAPs in Figure 3c. For *type 1* DAP spectra, where both donors and acceptors are located in the same lattice site, we inferred the possible DA pairs here to be $O_B^{(H)}\text{--anti}^{(E)}$ (~ 2.411 eV), $H_N^{(F)}\text{--}C_N^{(H)}$ (~ 2.18 eV), $H_N^{(F)}\text{--}O_N^{(H)}$ (~ 1.95 eV), $O_B^{(H)}\text{--}V_B^{(E)}$ (~ 1.708 eV), and $H_N^{(F)}\text{--}H_N^{(E)}$ (~ 1.430 eV). In the *type 2* DAP spectra listed in Figure S10, where donors and acceptors occupy the different lattice sites, the possible DA pairs are $H_N^{(F)}\text{--}V_B^{(H)}$ (~ 2.392 eV), $O_B^{(H)}\text{--}H_N^{(E)}$ (~ 2.215 eV), $\text{anti}^{(F)}\text{--}O_B^{(H)}$ (~ 1.978 eV), $\text{anti}^{(F)}\text{--}O_B^{(H)}$ (~ 1.691 eV), and $V_N^{(H)}\text{--}O_B^{(H)}$ (~ 1.408 eV). (V denotes the vacancy defects.) Here the SPE induced by the DAP transition mechanism in hBN provides a new way to understand the dense SPEs in semiconductors and opens a new way to produce single-photon sources for quantum technology. Because the defect-induced SPEs have also been observed in other emerging materials, such as transition-metal dichalcogenides^{40,41} and perovskite,⁴² the observation of DAP quantum emitters in these materials is expected.

■ TEMPERATURE DEPENDENCE OF THE DAP LINES

Next, we investigated the behavior of DAP lines at higher temperatures. These dense SPE lines become weaker at elevated temperatures, as shown in Figure 4a. When the temperature increases to ~ 160 K, some of the dense peaks vanish and cannot be individually resolved from each other. This result may be explained by considering the thermal effects on the fine structures and the binding energies of the ground states of the donor/acceptor. At a higher temperature, phonons broaden the luminescence lines; that is, when the energy difference between two peaks is smaller than the line width induced by thermal perturbation at the corresponding temperatures, they cannot be distinguished. On one hand, the

thermal energy of the crystal may free the originally paired donor and acceptor with a large R_m and reduce the number of peaks at higher temperatures. On the other hand, with temperature increasing, the thermal energy is big enough to approach the binding energies of the DAP. As a result, the probability of DAP transitions is greatly reduced, and other mechanisms such as the transition between the excited states and the ground states of defects dominate the fluorescence process.

We fit one representative PL peak from 4 to 160 K and plotted the temperature dependence of the extracted line widths and ZPL positions, as shown in Figure 4b. Because of the phonon effects at higher temperatures, the line shape shows a change from a Gaussian shape to a Lorentzian shape, consistent with our following analysis. At low temperatures, the PL ZPL is usually dominated by inhomogeneous broadening induced by spectral diffusion, exhibiting a Gaussian shape, whereas as the temperature increases, homogeneous broadening induced by phonons starts to dominate, leading to a Lorentzian shape at higher temperatures.^{43,44} From 4 to 160 K, the line widths show a T^3 temperature dependence, consistent with previous results.^{10,45–47} We found most of these DAP PL lines follow such a temperature dependence, as shown in Figure S11. Furthermore, most of the ZPL positions can be well described by using the O'Donnell equation.⁴⁸ This suggests that electron–phonon coupling plays an important role in the broadening and red shift of the DAP lines.

■ CONCLUSIONS

We demonstrated that the DAP transition mechanism could be one of the origins for the wide spectral viability of SPEs in hBN. These results indicate that an SPE on demand can be obtained by filtering the PL lines induced by the DAP transition or designing the distance of the DAP. Our work provides a fundamentally new understanding of hBN SPEs and opens a door to achieve supercontinuum single photon sources on one monolithic hBN sample. In addition, it also hints that the DAP mechanism should be an alternative way to produce quantum emitters in other semiconductors with efficient DAP emissions, such as silicon, silicon carbide, diamond, and other compound semiconductors.

EXPERIMENT METHODS

Photoluminescence Measurement. PL spectra measurements were undertaken in backscattering geometry with a Jobin-Yvon HR800 system equipped with a liquid-nitrogen-cooled charge-coupled detector. The samples were cooled by a Montana cryostat system. A 50× long-working-distance objective lens (NA = 0.5) and both 600 and 2400 lines mm⁻¹ gratings were used for the PL measurements at low temperatures. The highest resolution for our system with a 2400 lines mm⁻¹ grating was ~40 μeV.

Second-Order Correlation Function Measurement. The second-order correlation function measurement was carried out by using a home-built Hanbury–Brown–Twiss (HBT) setup. Two silicon avalanche photodiodes (APDs) were used to count photons. The 590 nm bandpass and 690 nm bandpass filters combined with a grating monochromator (1200 lines mm⁻¹) were used during the autocorrelation measurements.

ASSOCIATED CONTENT

Supporting Information

The Supporting Information is available free of charge at <https://pubs.acs.org/doi/10.1021/acs.nanolett.1c04647>.

DFT calculation details. Spectra and $g^{(2)}(\tau)$ measurements for more hBN samples (Figures S1 and S2). Temporal evolution of different emitters under continuous illumination at 4 K (Figure S3). Enlarged calculated type 1 DAP lines (Figure S4). Calculated type 1 DAP lines based on different $|E_D - E_A|$ (Figure S5). Calculated type 1 DAP lines for different samples (Figure S6). Calculation of type 2 DAPs (Figure S7). R_m -dependent DAP lifetimes (Figure S8). Band structure and energy level of defects for the monolayer hBN calculated by DFT (Figure S9). $|E_D - E_A|$ of different type 2 DAPs (Figure S10). Temperature dependence of line width and energy of different PL peaks (Figure S11) (PDF)

AUTHOR INFORMATION

Corresponding Authors

Igor Aharonovich – School of Mathematical and Physical Sciences, University of Technology Sydney, New South Wales 2007, Australia; ARC Centre of Excellence for Transformative Meta-Optical Systems, Faculty of Science University of Technology Sydney, New South Wales 2007, Australia; orcid.org/0000-0003-4304-3935; Email: igor.aharonovich@uts.edu.au

Weibo Gao – Division of Physics and Applied Physics, School of Physical and Mathematical Sciences, Nanyang Technological University, 637371, Singapore; orcid.org/0000-0003-3971-621X; Email: wbgao@ntu.edu.sg

Jun Zhang – State Key Laboratory of Superlattices and Microstructures, Institute of Semiconductors, Chinese Academy of Sciences, Beijing 100083, China; Center of Materials Science and Optoelectronics Engineering, University of Chinese Academy of Sciences, Beijing 100049, China; Beijing Academy of Quantum Information Science, Beijing 100193, China; CAS Center of Excellence in Topological Quantum Computation, University of Chinese Academy of Sciences, Beijing 101408, China; orcid.org/0000-0002-9831-6796; Email: zhangwill@semi.ac.cn

Authors

Qinghai Tan – State Key Laboratory of Superlattices and Microstructures, Institute of Semiconductors, Chinese Academy of Sciences, Beijing 100083, China; Center of Materials Science and Optoelectronics Engineering, University of Chinese Academy of Sciences, Beijing 100049, China; Division of Physics and Applied Physics, School of Physical and Mathematical Sciences, Nanyang Technological University, 637371, Singapore; orcid.org/0000-0003-4808-4795

Jia-Min Lai – State Key Laboratory of Superlattices and Microstructures, Institute of Semiconductors, Chinese Academy of Sciences, Beijing 100083, China; Center of Materials Science and Optoelectronics Engineering, University of Chinese Academy of Sciences, Beijing 100049, China

Xue-Lu Liu – State Key Laboratory of Superlattices and Microstructures, Institute of Semiconductors, Chinese Academy of Sciences, Beijing 100083, China; Center of Materials Science and Optoelectronics Engineering, University of Chinese Academy of Sciences, Beijing 100049, China

Dan Guo – State Key Laboratory of Superlattices and Microstructures, Institute of Semiconductors, Chinese Academy of Sciences, Beijing 100083, China; Center of Materials Science and Optoelectronics Engineering, University of Chinese Academy of Sciences, Beijing 100049, China

Yongzhou Xue – State Key Laboratory of Superlattices and Microstructures, Institute of Semiconductors, Chinese Academy of Sciences, Beijing 100083, China; Center of Materials Science and Optoelectronics Engineering, University of Chinese Academy of Sciences, Beijing 100049, China

Xiuming Dou – State Key Laboratory of Superlattices and Microstructures, Institute of Semiconductors, Chinese Academy of Sciences, Beijing 100083, China; Center of Materials Science and Optoelectronics Engineering, University of Chinese Academy of Sciences, Beijing 100049, China; orcid.org/0000-0002-4538-2087

Bao-Quan Sun – State Key Laboratory of Superlattices and Microstructures, Institute of Semiconductors, Chinese Academy of Sciences, Beijing 100083, China; Center of Materials Science and Optoelectronics Engineering, University of Chinese Academy of Sciences, Beijing 100049, China

Hui-Xiong Deng – State Key Laboratory of Superlattices and Microstructures, Institute of Semiconductors, Chinese Academy of Sciences, Beijing 100083, China; Center of Materials Science and Optoelectronics Engineering, University of Chinese Academy of Sciences, Beijing 100049, China; orcid.org/0000-0003-2155-8727

Ping-Heng Tan – State Key Laboratory of Superlattices and Microstructures, Institute of Semiconductors, Chinese Academy of Sciences, Beijing 100083, China; Center of Materials Science and Optoelectronics Engineering, University of Chinese Academy of Sciences, Beijing 100049, China; Beijing Academy of Quantum Information Science, Beijing 100193, China; CAS Center of Excellence in Topological Quantum Computation, University of Chinese Academy of Sciences, Beijing 101408, China; orcid.org/0000-0001-6575-1516

Complete contact information is available at: <https://pubs.acs.org/doi/10.1021/acs.nanolett.1c04647>

Author Contributions

Q.T. and J.-M.L. contributed equally. J.Z. and Q.T. conceived the ideas. Q.T., P.-H.T., and J.Z. designed the experiments.

Q.T. and X.-L.L. prepared the samples. Q.T., Y.X., and X.D. performed experiments. D.G. and H.-X.D. performed the DFT calculations. Q.T., J.-M.L., W.G., I.A., and J.Z. analyzed the data and wrote the manuscript with input from all authors.

Notes

The authors declare no competing financial interest.

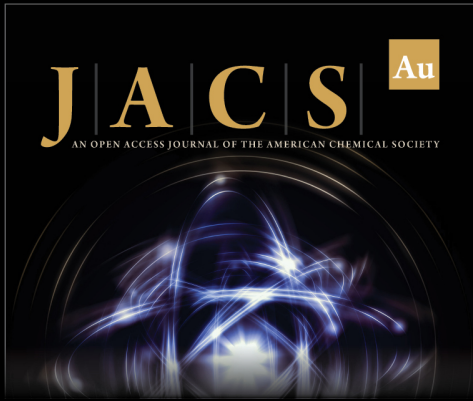
ACKNOWLEDGMENTS

J.Z. acknowledges support from the National Basic Research Program of China (grant no. 2017YFA0303401, 2016YFA0301200), Beijing Natural Science Foundation (JQ18014), and Strategic Priority Research Program of Chinese Academy of Sciences (grant no. XDB28000000) and CAS Interdisciplinary Innovation team. W.G. acknowledges the Singapore National Research Foundation and DSO National Laboratories under the QEP grants NRF2021-QEP2-03-P01, 2019-0643 (QEP-P2), and 2019-1321 (QEP-P3), CRP award nos. NRF-CRP21-2018-0007, NRF-CRP22-2019-0004, and NRF-CRP23-2019-0002, and the Singapore Ministry of Education (MOE2016-T3-1-006 (S)). I.A. acknowledges the financial support from the Australian Research Council (via CE200100010).

REFERENCES

- (1) Wang, G.; Chernikov, A.; Glazov, M. M.; Heinz, T. F.; Marie, X.; Amand, T.; Urbaszek, B. Colloquium: Excitons in atomically thin transition metal dichalcogenides. *Rev. Mod. Phys.* **2018**, *90* (2), 021001.
- (2) Lai, J.-M.; Xie, Y.-R.; Zhang, J. Detection of electron-phonon coupling in two-dimensional materials by light scattering. *Nano Res.* **2021**, *14* (6), 1711–1733.
- (3) Liu, X.; Hersam, M. C. 2D materials for quantum information science. *Nat. Rev. Mater.* **2019**, *4* (10), 669–684.
- (4) Ren, S.; Tan, Q.; Zhang, J. Review on the quantum emitters in two-dimensional materials. *J. Semicond.* **2019**, *40* (7), 071903.
- (5) Tran, T. T.; Bray, K.; Ford, M. J.; Toth, M.; Aharonovich, I. Quantum emission from hexagonal boron nitride monolayers. *Nat. Nanotechnol.* **2016**, *11* (1), 37–41.
- (6) Jungwirth, N. R.; Calderon, B.; Ji, Y.; Spencer, M. G.; Flatté, M. E.; Fuchs, G. D. Temperature Dependence of Wavelength Selectable Zero-Phonon Emission from Single Defects in Hexagonal Boron Nitride. *Nano Lett.* **2016**, *16* (10), 6052–6057.
- (7) Kianinia, M.; Regan, B.; Tawfik, S. A.; Tran, T. T.; Ford, M. J.; Aharonovich, I.; Toth, M. Robust Solid-State Quantum System Operating at 800 K. *ACS Photonics* **2017**, *4* (4), 768–773.
- (8) Exarhos, A. L.; Hopper, D. A.; Grote, R. R.; Alkuskas, A.; Bassett, L. C. Optical Signatures of Quantum Emitters in Suspended Hexagonal Boron Nitride. *ACS Nano* **2017**, *11* (3), 3328–3336.
- (9) Li, X.; Shepard, G. D.; Cupo, A.; Camporeale, N.; Shayan, K.; Luo, Y.; Meunier, V.; Strauf, S. Nonmagnetic Quantum Emitters in Boron Nitride with Ultranarrow and Sideband-Free Emission Spectra. *ACS Nano* **2017**, *11* (7), 6652–6660.
- (10) Jungwirth, N. R.; Fuchs, G. D. Optical Absorption and Emission Mechanisms of Single Defects in Hexagonal Boron Nitride. *Phys. Rev. Lett.* **2017**, *119* (5), 057401.
- (11) Grosso, G.; Moon, H.; Lienhard, B.; Ali, S.; Efetov, D. K.; Furchi, M. M.; Jarillo-Herrero, P.; Ford, M. J.; Aharonovich, I.; Englund, D. Tunable and high-purity room temperature single-photon emission from atomic defects in hexagonal boron nitride. *Nat. Commun.* **2017**, *8* (1), 705.
- (12) Xue, Y.; Wang, H.; Tan, Q.; Zhang, J.; Yu, T.; Ding, K.; Jiang, D.; Dou, X.; Shi, J.-j.; Sun, B.-q. Anomalous Pressure Characteristics of Defects in Hexagonal Boron Nitride Flakes. *ACS Nano* **2018**, *12* (7), 7127–7133.
- (13) Gao, X.; Jiang, B.; Llacsahuanga Allcca, A. E.; Shen, K.; Sadi, M. A.; Solanki, A. B.; Ju, P.; Xu, Z.; Upadhyaya, P.; Chen, Y. P.; Bhave, S. A.; Li, T. High-Contrast Plasmonic-Enhanced Shallow Spin Defects in Hexagonal Boron Nitride for Quantum Sensing. *Nano Lett.* **2021**, *21* (18), 7708–7714.
- (14) Gottscholl, A.; Kianinia, M.; Soltamov, V.; Orlinskii, S.; Mamin, G.; Bradac, C.; Kasper, C.; Krambrock, K.; Sperlich, A.; Toth, M.; Aharonovich, I.; Dyakonov, V. Initialization and read-out of intrinsic spin defects in a van der Waals crystal at room temperature. *Nat. Mater.* **2020**, *19* (5), 540–545.
- (15) Liu, W.; Li, Z.-P.; Yang, Y.-Z.; Yu, S.; Meng, Y.; Wang, Z.-A.; Li, Z.-C.; Guo, N.-J.; Yan, F.-F.; Li, Q.; Wang, J.-F.; Xu, J.-S.; Wang, Y.-T.; Tang, J.-S.; Li, C.-F.; Guo, G.-C. Temperature-Dependent Energy-Level Shifts of Spin Defects in Hexagonal Boron Nitride. *ACS Photonics* **2021**, *8* (7), 1889–1895.
- (16) Tawfik, S. A.; Ali, S.; Fronzi, M.; Kianinia, M.; Tran, T. T.; Stampfl, C.; Aharonovich, I.; Toth, M.; Ford, M. J. First-principles investigation of quantum emission from hBN defects. *Nanoscale* **2017**, *9* (36), 13575–13582.
- (17) Chejanovsky, N.; Rezaei, M.; Paolucci, F.; Kim, Y.; Rendler, T.; Rouabeih, W.; Fávoro de Oliveira, F.; Herlinger, P.; Denisenko, A.; Yang, S.; Gerhardt, I.; Finkler, A.; Smet, J. H.; Wrachtrup, J. Structural Attributes and Photodynamics of Visible Spectrum Quantum Emitters in Hexagonal Boron Nitride. *Nano Lett.* **2016**, *16* (11), 7037–7045.
- (18) Zibrov, A. A.; Kometter, C.; Zhou, H.; Spanton, E. M.; Taniguchi, T.; Watanabe, K.; Zaletel, M. P.; Young, A. F. Tunable interacting composite fermion phases in a half-filled bilayer-graphene Landau level. *Nature* **2017**, *549* (7672), 360–364.
- (19) Hayee, F.; Yu, L.; Zhang, J. L.; Ciccarino, C. J.; Nguyen, M.; Marshall, A. F.; Aharonovich, I.; Vučković, J.; Narang, P.; Heinz, T. F.; Dionne, J. A. Revealing multiple classes of stable quantum emitters in hexagonal boron nitride with correlated optical and electron microscopy. *Nat. Mater.* **2020**, *19* (5), 534–539.
- (20) Zhang, H.; Lan, M.; Tang, G.; Chen, F. L.; Shu, Z. W.; Chen, F. X.; Li, M. Discrete color centers in two-dimensional hexagonal boron nitride induced by fast neutron irradiation. *J. Mater. Chem. C* **2019**, *7* (39), 12211–12216.
- (21) Comtet, J.; Glushkov, E.; Navikas, V.; Feng, J.; Babenko, V.; Hofmann, S.; Watanabe, K.; Taniguchi, T.; Radenovic, A. Wide-Field Spectral Super-Resolution Mapping of Optically Active Defects in Hexagonal Boron Nitride. *Nano Lett.* **2019**, *19* (4), 2516–2523.
- (22) Fournier, C.; Plaud, A.; Roux, S.; Pierret, A.; Rosticher, M.; Watanabe, K.; Taniguchi, T.; Buil, S.; Quelin, X.; Barjon, J.; Hermier, J. P.; Delteil, A. Position-controlled quantum emitters with reproducible emission wavelength in hexagonal boron nitride. *Nat. Commun.* **2021**, *12* (1), 3779.
- (23) Uddin, M. R.; Li, J.; Lin, J. Y.; Jiang, H. X. Probing carbon impurities in hexagonal boron nitride epilayers. *Appl. Phys. Lett.* **2017**, *110* (18), 182107.
- (24) Gao, S.; Chen, H.-Y.; Bernardi, M. Radiative properties of quantum emitters in boron nitride from excited state calculations and Bayesian analysis. *npj Comput. Mater.* **2021**, *7* (1), 85.
- (25) Sajid, A.; Reimers, J. R.; Kobayashi, R.; Ford, M. J. Theoretical spectroscopy of the $V_{\text{N}}\text{N}_{\text{B}}$ defect in hexagonal boron nitride. *Phys. Rev. B* **2020**, *102* (14), 144104.
- (26) Sajid, A.; Reimers, J. R.; Ford, M. J. Defect states in hexagonal boron nitride: Assignments of observed properties and prediction of properties relevant to quantum computation. *Phys. Rev. B* **2018**, *97* (6), 064101.
- (27) Tajima, M.; Iwai, T.; Toyota, H.; Binetti, S.; Macdonald, D. Fine Structure Due to Donor–Acceptor Pair Luminescence in Compensated Si. *Appl. Phys. Express* **2010**, *3* (7), 071301.
- (28) Schmid, W.; Nieper, U.; Weber, J. Donor-acceptor pair spectra in Si: In LPE-layers. *Solid State Commun.* **1983**, *45* (12), 1007–1011.
- (29) Sun, J. W.; Ivanov, I. G.; Juillaguet, S.; Camassel, J. Splitting of type-I (N-B, P-Al) and type-II (N-Al, N-Ga) donor-acceptor pair spectra in 3C-SiC. *Phys. Rev. B* **2011**, *83* (19), 195201.
- (30) Choyke, W. J.; Patrick, L. Luminescence of Donor-Acceptor Pairs in Cubic SiC. *Phys. Rev. B* **1970**, *2* (12), 4959–4965.

- (31) Dischler, B.; Rothemund, W.; Wild, C.; Locher, R.; Biebl, H.; Koidl, P. Resolved donor-acceptor pair-recombination lines in diamond luminescence. *Phys. Rev. B* **1994**, *49* (3), 1685–1689.
- (32) Merz, J. L.; Nassau, K.; Shiever, J. W. Pair Spectra and the Shallow Acceptors in ZnSe. *Phys. Rev. B* **1973**, *8* (4), 1444–1452.
- (33) Thomas, D. G.; Gershenson, M.; Trumbore, F. A. Pair Spectra and "Edge" Emission in Gallium Phosphide. *Phys. Rev.* **1964**, *133* (1A), A269–A279.
- (34) Thomas, D. G.; Hopfield, J. J.; Augustyniak, W. M. Kinetics of Radiative Recombination at Randomly Distributed Donors and Acceptors. *Phys. Rev.* **1965**, *140* (1A), A202–A220.
- (35) Dean, P. J.; Schönherr, E. G.; Zetterstrom, R. B. Pair Spectra Involving the Shallow Acceptor Mg in GaP. *J. Appl. Phys.* **1970**, *41* (8), 3475–3479.
- (36) Kobr, L.; Gardner, D. M.; Smeigh, A. L.; Dyar, S. M.; Karlen, S. D.; Carmieli, R.; Wasielewski, M. R. Fast Photodriven Electron Spin Coherence Transfer: A Quantum Gate Based on a Spin Exchange J-Jump. *J. Am. Chem. Soc.* **2012**, *134* (30), 12430–12433.
- (37) Wu, Y.; Zhou, J.; Nelson, J. N.; Young, R. M.; Krzyaniak, M. D.; Wasielewski, M. R. Covalent Radical Pairs as Spin Qubits: Influence of Rapid Electron Motion between Two Equivalent Sites on Spin Coherence. *J. Am. Chem. Soc.* **2018**, *140* (40), 13011–13021.
- (38) Auburger, P.; Gali, A. Towards ab initio identification of paramagnetic substitutional carbon defects in hexagonal boron nitride acting as quantum bits. *Phys. Rev. B* **2021**, *104* (7), 075410.
- (39) Cassabois, G.; Valvin, P.; Gil, B. Hexagonal boron nitride is an indirect bandgap semiconductor. *Nat. Photonics* **2016**, *10* (4), 262–266.
- (40) So, J.-P.; Jeong, K.-Y.; Lee, J. M.; Kim, K.-H.; Lee, S.-J.; Huh, W.; Kim, H.-R.; Choi, J.-H.; Kim, J. M.; Kim, Y. S.; Lee, C.-H.; Nam, S.; Park, H.-G. Polarization Control of Deterministic Single-Photon Emitters in Monolayer WSe₂. *Nano Lett.* **2021**, *21* (3), 1546–1554.
- (41) Iff, O.; Tedeschi, D.; Martín-Sánchez, J.; Moczala-Dusanowska, M.; Tongay, S.; Yumigeta, K.; Taboada-Gutiérrez, J.; Savaresi, M.; Rastelli, A.; Alonso-González, P.; Höfling, S.; Trotta, R.; Schneider, C. Strain-Tunable Single Photon Sources in WSe₂ Monolayers. *Nano Lett.* **2019**, *19* (10), 6931–6936.
- (42) Huo, C.; Fong, C. F.; Amara, M.-R.; Huang, Y.; Chen, B.; Zhang, H.; Guo, L.; Li, H.; Huang, W.; Diederichs, C.; Xiong, Q. Optical Spectroscopy of Single Colloidal CsPbBr₃ Perovskite Nanoplatelets. *Nano Lett.* **2020**, *20* (5), 3673–3680.
- (43) Muller, T.; Aharonovich, I.; Wang, Z.; Yuan, X.; Castelletto, S.; Praver, S.; Atature, M. Phonon-induced dephasing of chromium color centers in diamond. *Phys. Rev. B* **2012**, *86* (19), 195210.
- (44) Neu, E.; Hepp, C.; Hauschild, M.; Gsell, S.; Fischer, M.; Sternschulte, H.; Steinmüller-Nethl, D.; Schreck, M.; Becher, C. Low-temperature investigations of single silicon vacancy colour centres in diamond. *New J. Phys.* **2013**, *15* (4), 043005.
- (45) Sontheimer, B.; Braun, M.; Nikolay, N.; Sadzak, N.; Aharonovich, I.; Benson, O. Photodynamics of quantum emitters in hexagonal boron nitride revealed by low-temperature spectroscopy. *Phys. Rev. B* **2017**, *96* (12), 121202.
- (46) Hizhnyakov, V.; Kaasik, H.; Sildos, I. Zero-phonon lines: The effect of a strong softening of elastic springs in the excited state. *Phys. Status Solidi B* **2002**, *234* (2), 644–653.
- (47) Hizhnyakov, V.; Boltrushko, V.; Kaasik, H.; Sildos, I. Strong Jahn–Teller effect in the excited state: Anomalous temperature dependence of the zero-phonon line. *J. Chem. Phys.* **2003**, *119* (12), 6290–6295.
- (48) O'Donnell, K. P.; Chen, X. Temperature dependence of semiconductor band gaps. *Appl. Phys. Lett.* **1991**, *58* (25), 2924–2926.



JACS Au
AN OPEN ACCESS JOURNAL OF THE AMERICAN CHEMICAL SOCIETY

Editor-in-Chief
Prof. Christopher W. Jones
Georgia Institute of Technology, USA

Open for Submissions 

pubs.acs.org/jacsau  ACS Publications
Most Trusted. Most Cited. Most Read.